EurJIC
European Journal of Inorganic Chemistry

Research Article
doi.org/10.1002/ejic.202400108

Chemistry Europe
European Chemical Societies Publishing

www.eurjic.org

Electronic Effect of the $[Au(PPh_3)]^+$ Fragment in the Stabilization of Imidazolium Salts and the Destabilization of NHCs

Miguel A. Rosero-Mafla,[a, b] Manuel N. Chaur,[a, b] Cesar A. Mujica-Martinez,[c] Vanesa Fernández-Moreira,[d] Jhon Zapata-Rivera,[a, b] M. Concepción Gimeno,*[d] and Renso Visbal*[a, b]

Dedicated to Prof. Esperanza Galarza de Becerra and Prof. Alberto Bolaños Rivera for their contributions to the field of Inorganic Chemistry and to the Department of Chemistry at the Universidad del Valle.

This work presents the synthesis and characterization of mono- (**1**) and di-nuclear (**2**) imidazolium salts stabilized by $[AuPPh_3]^+$ fragments. The presence of the gold moiety induces a significant decrease in the carbenic proton's acidic character (high pKa). This high stability is consistent with the pronounced instability of the conjugate bases obtained through deprotonation using strong bases. The formation of carbene species is accompanied by the identification of a 1,2-rearrangement process in which a preference for the *C*-bound species over the *N*-bound species is observed. Experimental techniques such as NMR, single-crystal X-ray diffraction analysis, mass spectrometry, and computational calculations are employed to investigate the reactivity exhibited by the imidazolium salts. Additionally, the electrochemical properties of the two imidazolium salts were also investigated. This study reveals that both species **1** and **2** display two cathodic peaks which are related to two electrochemical irreversible reduction events. The results obtained from both experimental and theoretical studies of this system reveal a strong tendency of the $[AuPPh_3]^+$ fragment to stabilize imidazolium salts. Additionally, they demonstrate the preference of this fragment for *C*-bound species over *N*-bound ones, with the former proving to be highly unstable even under severe conditions of air and moisture exclusion.

Introduction

The great impact of *N*-heterocyclic carbenes (NHCs) in chemical sciences is well supported by the vast number of papers published in many research fields.[1–4] The increasing tendency of the use of such ligands in many important applications is mainly due to their great versatility and stability towards metal and non-metal coordination compounds.[5–7] In addition to the stability resulting from the electronic delocalization in the NCHN moiety, the electron pair is stabilized by the relatively easy electronic modulation and the steric effect induced by the functional groups anchored in the nitrogen atoms.[5] The design of an appropriate imidazolium salt used as a precursor for the synthesis of carbene ligands takes a crucial role. Most of these precursors contain alkyl or aryl groups adjacent to the N atoms, which promote electronic states needed for the stabilization of the sp^2 hybridized lone pair.[8] There are a lot of experimental and theoretical studies focused on the understanding of the characteristics and behavior of these "classical" NHC ligands.[9–12] On the other hand, the synthesis and characterization of imidazolium salts and NHC ligands containing anchored motifs different from alkyl or aryl groups are poorly described or reported.[12–15] For instance, the incorporation of a metal center into the nitrogen atoms causes significant differences in the overlapping of the orbitals involved in the stabilization of the NHC ligand.[16,17]

[a] *MSc. M. A. Rosero-Mafla, Prof. Dr. M. N. Chaur, Dr. J. Zapata-Rivera, Dr. R. Visbal*
Departamento de Química
Facultad de Ciencias Naturales y Exactas, Universidad del Valle
A.A. 25360 Cali (Colombia)
E-mail: renso.visbal@correounivalle.edu.co

[b] *MSc. M. A. Rosero-Mafla, Prof. Dr. M. N. Chaur, Dr. J. Zapata-Rivera, Dr. R. Visbal*
Centro de Excelencia en Nuevos Materiales (CENM)
Universidad del Valle
A.A. 25360 Cali (Colombia)

[c] *Prof. Dr. C. A. Mujica-Martinez*
Departamento de Química
Universidad de Nariño
520002 San Juan de Pasto, Nariño, Colombia

[d] *Dr. V. Fernández-Moreira, Prof. Dr. M. C. Gimeno*
Departamento de Química Inorgánica
Instituto de Síntesis Química y Catálisis Homogénea (ISQCH) CSIC-Universidad de Zaragoza
C/ Pedro Cerbuna 12, 50009 Zaragoza, Spain
E-mail: gimeno@unizar.es

Supporting information for this article is available on the WWW under https://doi.org/10.1002/ejic.202400108

Research Article
doi.org/10.1002/ejic.202400108

Crabtree and co-workers theoretically studied the effects of several metal fragments on the *C*-binding versus *N*-binding forms in imidazole derivatives (Scheme 1).[18] They found that *C*-bound imidazoles are predicted to be thermodynamically more stable than *N*-bound forms for several transition metals, especially, for the third-row metals, where the AuCl fragment, isolobal with the proton, showed a small relative energy of −2.0 kcal/mol in agreement with the small tendency of gold to stabilize M–C bonds over the M–N ones.[18] Despite this early report, there are few reports studying the effects of the coordination of gold centers in the stabilization of imidazolium salts and NHCs.

In 2007, Ruiz and co-workers studied the based-promoted isomerization process in several heterobimetallic complexes containing the $[Au(PPh_3)]^+$ fragment (Scheme 2a). They found that the addition of $[AuCl(PPh_3)]$ to the starting Mn-carbene species **I** in the presence of KOH affords species **III**, in which the heterobimetallic species **II** was proposed as an intermediate that undergoes an isomerization process.[19] Later, computational studies showed that an η^2-imidazol-2-yl bridging ligand was found to be the key intermediate in this base-promoted transmetallation process involving protic *N*-heterocyclic carbenes.[20]

In subsequent related works, Riera and co-workers also found the same reactivity pattern, in which, the starting M-carbene species **IV** and **VI** (M = Re, Mo) displayed a clear tendency to stabilize the heterobimetallic complexes **V** and **VII** containing the NHC moiety *C*-bound to gold *vs.* *C*-bound to Re or Mo ones, which were proposed as a result of a tautomerization process (Scheme 2b–c).[16,17]

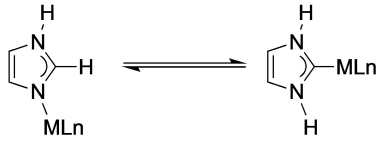

Scheme 1. Equilibrium promoted by the presence of a metal fragment in the imidazole.

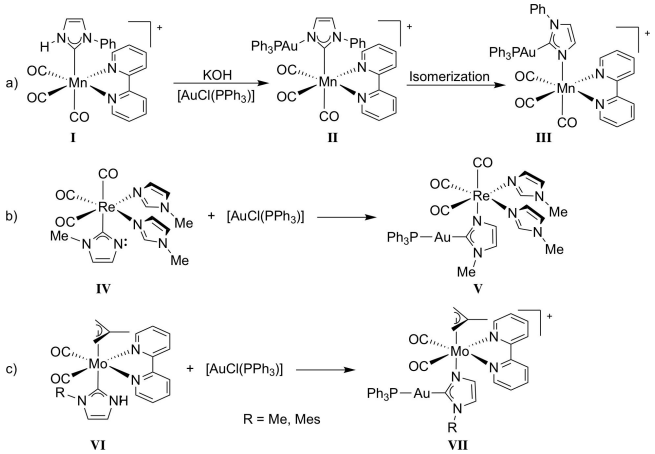

Scheme 2. Reactivity of different imidazole-containing complexes in the presence of $[AuCl(PPh_3)]$.

In this work, we study experimentally and computationally the effects of the $[Au(PPh_3)]^+$ fragment in the stabilization of imidazolium salts and the capacity of these derivatives to be used as precursors of *N*-heterocyclic carbenes.

Results and Discussion

Synthesis and Characterization

The preparation of gold-containing imidazolium salts was attempted following the synthesis described in Scheme 3 (top). The reaction of *N*-methyl imidazole with one equivalent of the gold derivative $[Au(OTf)(PPh_3)]$ in dichloromethane gives the gold imidazolium salt **1** after 2 h in a moderate yield (75%), isolated as a beige solid. The coordination of the nitrogen donor imidazole derivative is facilitated by the presence of a non-coordinating trifluoromethanesulfonate counteranion ($CF_3SO_3^-$ or OTf^-). As observed from the ^1H NMR spectra (Figures 1(top) and S1), there are significant differences when comparing to 1,3-dimethylimidazolium salt ($[IMe_2{-}H]^+$) previously reported[21,22] that are worth mentioning.

Besides the expected high-field signal at 3.89 ppm corresponding to the methyl group, two signals attributed to the protons at the C4 and C5 positions of the imidazole ring rise,

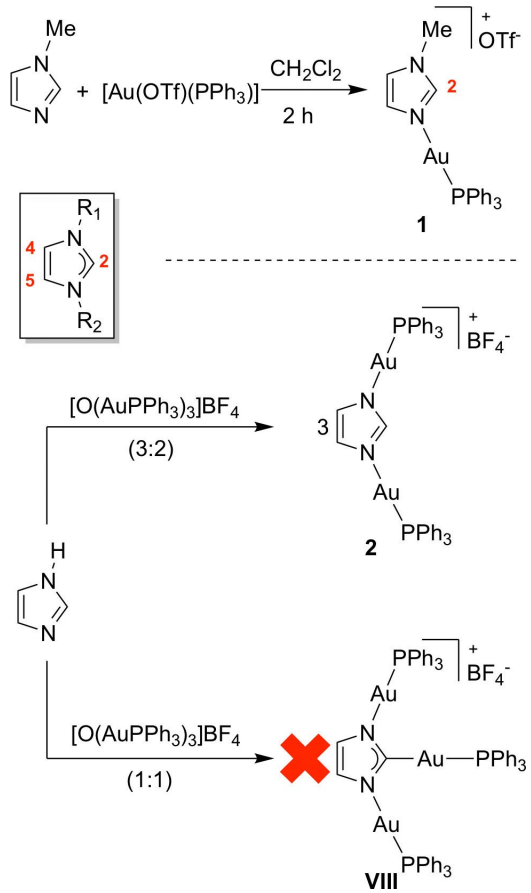

Scheme 3. Synthesis of the gold imidazolium salts **1** and **2** and attempts to prepare the NHC-gold carbene **VIII**.

Research Article
doi.org/10.1002/ejic.202400108

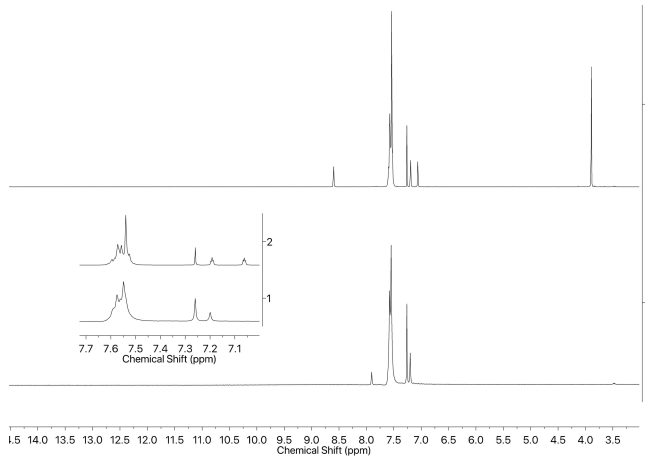

Figure 1. ^{1}H NMR spectra of compound **1** (Top) and compound **2** (Bottom) in $CDCl_3$.

indicating a reduction in symmetry of such ring in complex **1** as compared to that observed for a symmetric IMe_2 derivative. A multiplet in the aromatic region, integrating for 15 protons, confirms the presence of the triphenylphosphine group. Furthermore, the substitution of the alkyl group with the $[Au(PPh_3)]^+$ moiety induces a less shielding of the signal assigned to the C2-H proton, which appears at 8.60 ppm, as compared to the 1,3-dimethylimidazolium analog, where it is observed at approximately 9.08 ppm.[21] These observations align with the findings from the ^{13}C-{^{1}H}, ^{31}P-{^{1}H}, and ^{19}F NMR spectra acquired for compound **1**, which revealed the presence of an *N*-bonded $[Au(PPh_3)]^+$ fragment and a $CF_3SO_3^-$ anion. Additionally, in the ESI$^+$ mass spectrum, a molecular peak at 541.0 *m/z* exhibits an isotopic distribution characteristic of the $[M\text{-}OTf]^+$ fragment, resulting from the dissociation of imidazolium salt **1** in solution (see Figures S2–S5).

Traditionally, the oxonium ion $[O(AuPPh_3)_3]^+$, which possesses a similar basic character to acetylacetonate ($acac^-$), acetate (OAc^-), etc, has been used to incorporate $[Au(PPh_3)]^+$ fragments through a deprotonation process.[23,24] In this context, the reaction of 3 equivalents of imidazole with 2 equivalents of the gold-oxonium precursor $[O(AuPPh_3)_3]BF_4$ was carried out to afford the dinuclear complex **2** in a moderate yield (76%) after 2 hours in dichloromethane (Scheme 3 (bottom)). In agreement with the results obtained for compound **1**, the C2–H proton signal in complex **2** now appears at low frequencies (7.90 *vs.* 8.60 ppm) compared to that observed for compound **1** (Figure 1 (bottom) and S6). Additionally, the 1:30 ratio between the C2–H proton of the imidazole ring and the phenyl groups of the PPh_3 moieties suggests the presence of $[I(AuPPh_3)_2H]BF_4$. Again, a singlet at 31.72 ppm in the ^{31}P-{^{1}H} NMR and at −148.2 ppm in the ^{19}F spectra, and the identification of a peak at *m/z* = 985.1 in the MALDI$^+$ mass spectrum confirms the presence of a symmetrical imidazolium ring with two *N*-bonded phosphine-containing gold moieties (See Figures S7–S10).

To evaluate the capacity of $[O(AuPPh_3)_3]BF_4$ to incorporate a third $[Au(PPh_3)]^+$ fragment, thus forming the carbenic species **VIII**, the reaction using stoichiometric quantities of imidazole and $[O(AuPPh_3)_3]BF_4$ (1:1) was attempted. However, the analysis of the crude reaction by NMR spectroscopy revealed the formation of complex **2** and $[Au(PPh_3)_2]BF_4$ as byproducts. (Scheme 3). Once again, this could be associated with the lower Lewis acid character of **2** compared to traditional imidazolium salts, which exhibited a signal at 7.90 ppm corresponding to a much more shielded C2–H proton. Additionally, the absence of a coordinating anion such as halides, could be associated with the non-formation of intermediate species that plays a key role in the preparation of gold-NHC complexes when using weak bases.[25,26]

Suitable crystals for X-ray diffraction analysis were obtained for derivative **1**. The molecular structure is depicted in Figure 2. In agreement with the experimental data previously commented, compound **1** is an *N*-bound imidazole containing a $[Au(PPh_3)]^+$ fragment. As expected, the coordination around the gold center is almost lineal with an N2–Au1–P1 bond angle of 175.10(5)° and Au1–N2 and Au1–P1 bond distances of 2.0498(19) and 2.2329(6) Å, respectively (For more details see Tables S1–S2), which are in good agreement to those found for other analog imidazolium salts containing the gold(I)-triphenylphosphane fragment.[27] In addition, the geometry optimization calculations of compound **1**, including implicit solvent effects, reveal no significant deviation from the optimized structure regarding the X-ray structure (see Table S3). Additionally, in the crystal packing of compound **1** along the *a* axis, a significant contribution of the $[AuPPh_3]^+$ fragment was observed (Figure 3). For instance, the analysis of short contacts in the crystal packing revealed that the intermolecular interaction between imidazolium cations is primarily governed by the presence of C–H···π interactions from PPh_3 moieties, with a minor contribution from the $CF_3SO_3^-$ anions. This observation supports the idea of C–H···π interactions playing a key role in the molecular assembly in our system.[28]

Reactivity and Computational Studies

DFT-based calculations were conducted to explain the experimental findings (see the Supporting Information for computa-

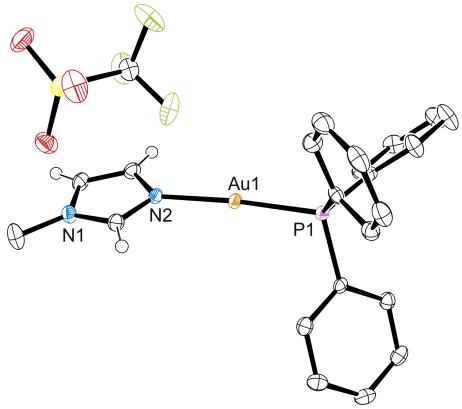

Figure 2. ORTEP representation (50% probability ellipsoids) of compound **1**. Most hydrogen atoms have been omitted for clarity.

Research Article
doi.org/10.1002/ejic.202400108

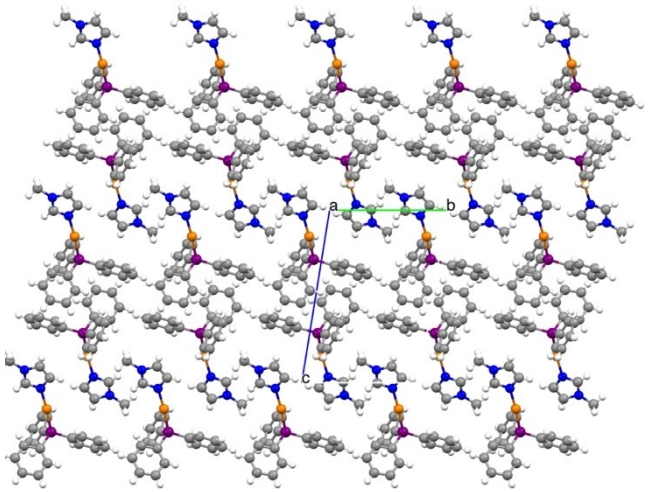

Figure 3. View along the *a*-axis of the crystal packing of **1**. The axes are represented as *a*, *b*, *c*. Anion molecules are omitted for clarity.

tional details). In line with the experiments, the calculated chemical shift showed a more shielded C2–H proton in complex **1** compared to the $[IMe_2–H]^+$ cation. Such behavior is probably caused by the larger values of shielding and spin-spin coupling constants imposed by the $[Au(PPh_3)]^+$ moiety. This can be related to a smaller value of the Natural Bond Orbital (NBO) charge of the C2–H proton (Table S5). The strong basicity of *N*-heterocyclic carbenes is deeply related to the relatively weak acidity of the C2 carbon of an imidazolium salt, which can undergo ionization leading to the corresponding singlet imidazol-2-yl carbene. Amyes and co-workers have studied the formation and stability of traditional NHCs in water, concluding that the carbon acid p*K*a of imidazolium cations in aqueous solution (21.2-23.8) are intermediate between those of the prototypical neutral carbonyl carbon acids such as acetone (pKa = 19.3) and ethyl acetate (pKa = 25.6).[29] According to this and the NMR experiments, the incorporation of the $[Au(PPh_3)]^+$ fragment favors a significant stabilization of the formed imidazolium salt (δ C2–H = 8.60 ppm), as compared to 1,3-dimethylimidazolium salt. The acidity of the C2–H proton has been also evaluated computationally in terms of pKa (see the SI for computational details). As shown in Table S6, the larger pKa value of compound **1** (44.2) compared to the $[IMe_2–H]^+$ derivative (31.8) indicates that the $[Au(PPh_3)]^+$ fragment decreases the acidity of the C2–H proton, and enhances the stability of the *N*-bound imidazole.

When comparing the ease deprotonation of the C2–H proton, the calculated pKa values indicate a decrease in the order IMe > **2** > **1** > IMe_2 which suggests that the metal complexation promotes a diminishing in the imidazole C2–H proton acidity. Here, a relationship between a smaller value of the NBO charge of the C2–H proton and a larger pKa value is also observed (Tables S5 and S6). Furthermore, the higher pKa value of compound **2** compared to compound **1** indicates greater stabilization of the *N*-bound imidazole due to the presence of an additional $[Au(PPh_3)]^+$ fragment.

N-heterocyclic carbenes are characterized by their relative stability compared to traditional carbenes, *e.g.* Fischer and Schrock.[30] In particular, stabilized imidazolylidenes and imidazolinylidenes as those reported by Arduengo,[21,22] have been extensively used in the preparation of a great variety of metal complexes through a transmetallation reaction or by *in situ* generation of the free carbene.[30] Unfortunately, none of these methods allowed the formation of any carbene complex. For instance, the use of metal precursors, known for their nucleophilic character, such as Ag_2O or $[Au(acac)(PPh_3)]$ does not promote the proton abstraction from the imidazolium salts (**1** or **2**), even at high temperatures, while the use of strong or weak bases such as *n*-BuLi, KHMDS, NaH, or K_2CO_3 with the subsequent addition of gold precursors ([AuCl(tht)] or $[Au(OTf)(PPh_3)]$) leads to the spontaneous decomposition to metallic gold.

To have a better idea about the behavior of the free carbene, generated from imidazoles containing the $[Au(PPh_3)]^+$ fragment, the reaction of compound **1** with NaH in deuterated acetonitrile was carried out in an NMR tube (Scheme 4). The results suggest that the generation of the free carbene was achieved, but as observed from the $^{31}P\{^1H\}$ NMR spectrum, there is a rearrangement process between the *N*-bounded (30.20 ppm) and *C*-bounded (37.99 ppm) forms (Figure 4). Although this migration process is in agreement with other reports,[16,17] in our case it is not enough to support the low stability presented for the free carbene after further addition of gold precursors.

Free energies of the different tautomers of compound **1**, as well as of the respective species **i** and **ii** arising from the deprotonation of derivative **1** were calculated, (see Table S7). The results indicate that before deprotonation, the *N*-bound imidazole (**i**) is 2.69 kcal/mol more stable than the *C*-bound tautomer, which is consistent with previously reported works.[18] However, after deprotonation, the *C*-bound species (**ii**) is

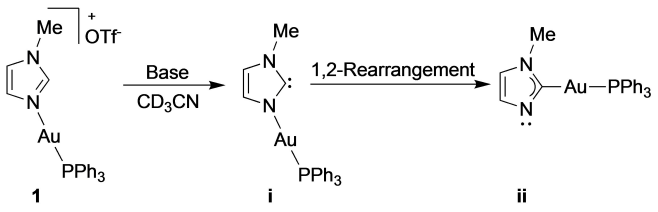

Scheme 4. Proposed 1,2-rearrangement process between species **i** and **ii** after proton abstraction of compound **1**.

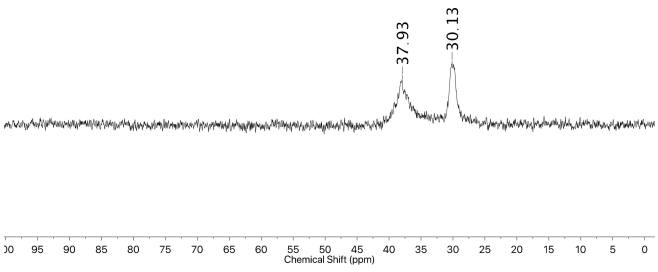

Figure 4. $^{31}P\{^1H\}$ NMR spectrum of compound **1** treated with NaH in CD_3CN.

thermodynamically more stable by 20.120 kcal/mol, which seems to be in contrast with a possible tautomerization process between the *C*-bound and *N*-bound forms. The calculated activation free energy of 13.026 kcal/mol is in line with a kinetically unfavorable process, reinforcing our prior construction. The observation of both species in the ^{31}P-{^{1}H} NMR spectrum can be attributed to the very slow transformation from the *N*-bound form to the *C*-bound one ($k = 1.76\times10^{3}$ s^{-1} at 298.15 K, assuming an unimolecular reaction in the framework of Eyring-Polányi approximation). Unfortunately, species **ii** is highly unstable and rapidly decomposed to metallic gold and other unknown gold derivatives.

To obtain mechanistic information about the 1,2-rearrangement process between species **i** (*N*-bound) and **ii** (*C*-bound), Wiberg bond indices[31] were calculated[32] (Table 1; for further computational details see the Supporting Information).

Wiberg bond indices allow to monitor bond changes by quantifying the electron population between two atoms. The values in Table 1 account for the changes in the electron population when the rearrangement from the *N*-bound (large B_{Au-N} and small B_{Au-C}) to the *C*-bound imidazole (large B_{Au-C} and small B_{Au-N}) takes place. In the TS the B_{Au-C} and B_{Au-N} values become more comparable. Noteworthy, the N–C bond strengthens when going from the *N*-bound to the *C*-bound imidazole. Evolution percentages of 41.13% and 43.72% were obtained for the Au–N and C–Au bonds, respectively, which indicate that at the transition state, the formation of the C–Au bond is more advanced than the breaking of the Au–N bond. These percentages agree with the obtained early transition state ($\delta B_{av} < 0.5$), which is also consistent with the exergonic nature of the tautomerization processes.[33] Despite the different evolution percentages, the Au–N bond breaking and the C–Au bond formation can be considered as a highly synchronous ($S > 0.9$) and concerted process.

Electrochemical Properties

The redox behavior of the gold(I)-based complexes **1** and **2** was studied by cyclic voltammetry (CV) and Osteryoung Square Wave Voltammetry (OSWV) at room temperature (for details see the Experimental section). Both compounds exhibit two reduction potentials. For complex **2** the first peak potential is cathodically shifted while the second peak is anodically shifted (see Figure 5) in agreement with the relative energy of the molecular orbitals for both compounds (Figure S18). No stable oxidation peaks are observed, although both compounds are very sensitive to oxidation since scanning farther than 1.0 V causes irreversible decomposition.

DFT calculations reveal that after the first reduction event of complex **1**, the additional electron is delocalized on the triphenylphosphine ligand (see Figure 7). Similarly, in the second reduction event, the ligand retains the additional electron with planarity loss of a phenyl ring of the $[Au(PPh_3)]^+$ fragment (Figure S14).

The CV of complex **2** (Figure 6) shows, similar to complex **1**, two cathodic peaks that are related to two electrochemically irreversible reduction events but, in this case, return waves are observed at −1.07 V and −1.60 V, respectively. For instance, for compound **2**, the first reduction potential is separated ~300 mV from the return peak wave which, in turn, is of lower intensity. Faster scan rates do not seem to give insight into any

Table 1. Calculated parameters associated with the chemical bonds involved in the rearrangement process after deprotonation of compound **1**.

Parameters[a]		Au–N	N–C	C–Au
B_j	*N*-bound imidazole	0.3785	1.3508	0.0788
	TS	0.2415	1.3959	0.3139
	C-bound imidazole	0.0454	1.4875	0.6165
δB_{av}		0.3928		
S		0.9199		

[a] Parameters: B_j are the Wiberg bond indices, δB_{av} is the average value of the bond indices, and *S* is the absolute synchronicity. TS = transition state.

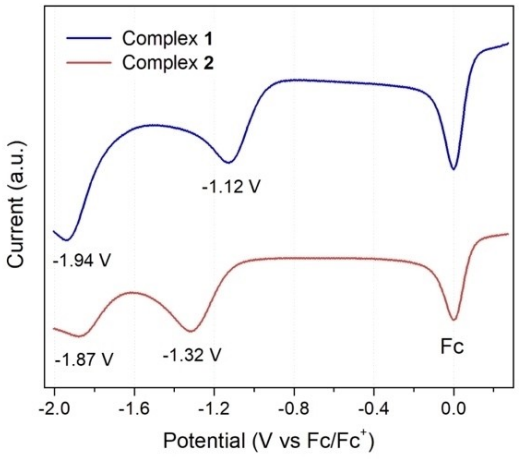

Figure 5. OSWV of complexes **1** (in blue) and **2** (in red) in (n-Bu_4NPF_6/CH_3CN with ferrocene as internal standard.

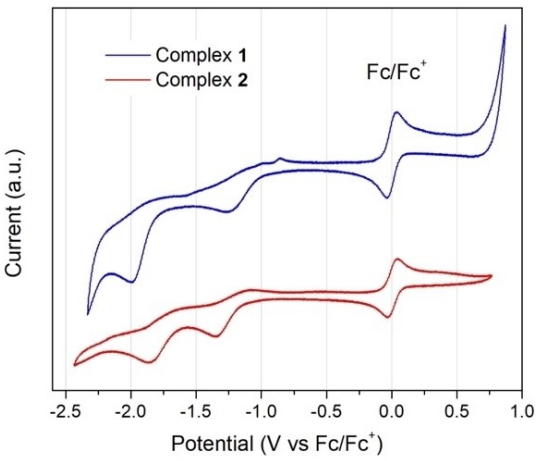

Figure 6. CV of complexes **1** (in blue) and **2** (in red) in (n-Bu_4NPF_6/CH_3CN with ferrocene as internal standard.

Research Article
doi.org/10.1002/ejic.202400108

reversibility. If we compare both complexes, the anion radical is easier accommodated in complex **1** (lower reduction peak potential) but more stabilized in complex **2**, probably due to the significant gold contribution in the LUMO for the former (Figures 7 and S14). This behavior, of complex **2**, indicates the stabilization effect of the second $[Au(PPh_3)]^+$ fragment and its capacity to withstand the electrical load. OSWV shows more clearly these two reduction events. The first cathodic peak of complex **2** is cathodically shifted compared to complex **1**, which suggests that the second $[Au(PPh_3)]^+$ fragment has an impact on the electronic structure; the LUMO of complex **2** increases its energy (Figure S18). Interestingly, Wiberg bond indices of the Au–N and Au–P bonds of complexes **1** and **2** suggest that after each reduction event, the former is weakened while the latter is strengthened (Table S9). The reversible behavior of complex **2** can be attributed to the second $[Au(PPh_3)]^+$ fragment, which is not affected in its geometry by the reduction events (see SOMO and HOMO in Figures S15–S17). Finally, the linear relationship between the current peaks (I_c) and the square root of the scan rate ($V^{1/2}$) indicates that all the electron transfer processes are controlled by diffusion (see Figures S12–S13).

Conclusions

Two new imidazolium salts containing the $[Au(PPh_3)]^+$ fragment were synthesized and characterized by NMR spectroscopy, X-ray diffraction analysis, mass spectrometry, and DFT-based calculations. The X-ray structure of compound **1** confirmed the presence of the gold(I) fragment bound to the nitrogen atom of the imidazolium ring. In this study, the effect of incorporating the gold fragment into imidazole derivatives was evaluated by NMR spectroscopy and theoretical calculations, revealing a significant decrease in the acid character of imidazolium salts **1** and **2** (larger pKa values) compared to traditional (dialkyl or diaryl) imidazolium salts. Additionally, the trend of the $[Au(PPh_3)]^+$ fragment to form *C*-bound species rather than *N*-bound was confirmed after the formation of the corresponding carbenic species. However, the *C*-bound species proved to be quite unstable, even under harsh conditions of air and moisture exclusion, exhibiting decomposition reactions into metallic gold and other unknown species in the reaction mixture. Finally, both mononuclear (**1**) and dinuclear (**2**) salts showed two cathodic peaks which are related to two electrochemically irreversible reduction events. These results together with those obtained from computational experiments are in good agreement with the marked stability *vs.* traditional imidazolium salts.

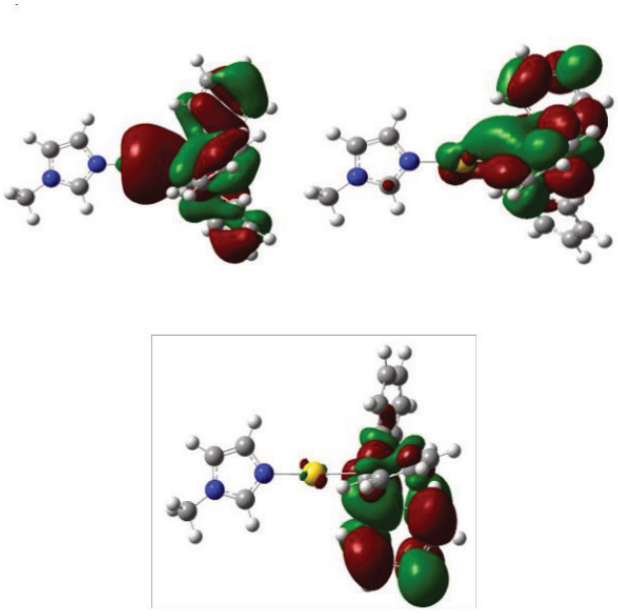

Figure 7. HOMO (top left) and LUMO (top right) of complex **1**. SOMO (bottom) of complex **1** after the first reduction event. *Colors*: carbon in grey, hydrogen in white, nitrogen in blue, gold in yellow, and phosphorous in orange. Orbitals depict an Isosurface of 0.02 $\left(e/a_0^3\right)^{1/2}$.

Experimental Section

Instrumentation: C, H, and N analyses were carried out with a PERKIN-ELMER 2400 microanalyzer. Mass spectra were recorded on a Bruker Microflex (MALDI-TOF). ^1H and $^{13}C\{^1H\}$-APT NMR, including 2D experiments, were recorded at room temperature on a BRUKER AVANCE 400 spectrometer (^1H, 400 MHz; ^{13}C, 100.6 MHz; ^{19}F, 376.5 MHz) or on a BRUKER AVANCE II 300 spectrometer (^1H, 300 MHz; ^{13}C, 75.5 MHz; ^{19}F, 282.3 MHz), with chemical shifts (ppm) reported relative to the solvent peaks of the deuterated solvent.[34]

Starting materials: All reactions were performed under air atmosphere and solvents were used as received without further purification or drying unless otherwise stated. Imidazole, N-methyl imidazole and bases were purchased from Sigma-Aldrich. Gold precursor $[O(AuPPh_3)_3]BF_4$ was prepared according to published procedures.[35] $[Au(OTf)(PPh_3)]$ was prepared from $[AuCl(PPh_3)]$[36] and AgOTf in dichloromethane in the molar ratio 1 : 1; the mixture was stirred for 1 h, and then the AgCl was filtered off and the solution containing $[Au(OTf)(PPh_3)]$ was used immediately.

Preparation of compound 1. A flask was charged with 103.5 mg (1.26 mmol) of N-methylimidazole, 20 mL of CH_2Cl_2, and 800 mg (1.30 mmol) of $[Au(OTf)(PPh_3)]$. After 2 h of stirring in dark, the mixture changed from colorless to pale-yellow. Then, the solution was evaporated to minimum volume under vacuum, and compound **1** was precipitated and washed with diethyl ether as a beige solid.

$[IMe(AuPPh_3)H]OTf$ (**1**). Yield: 0.6560 g (75 %) ^1H NMR ($CDCl_3$, 300 MHz, 294 K) δ 8.60 (s, 1H, H2, Im), 7.60-7.53 (m, 15H, Ph, PPh_3), 7.19 (m, 1H, H4, Im), 7.06 (m, 1H, H5, Im), 3.89 (s, CH_3). $^{13}C\{^1H\}$-APT NMR (CD_2Cl_2, 101 MHz, 294 K) δ 134.3 (d, J_{C-P} = 13.6 Hz, Ph, PPh_3), 132.4 (d, J_{C-P} = 13.6 Hz, Ph, PPh_3), 129.6 (d, J_{C-P} = 11.9 Hz, Ph, PPh_3), 128.2, (d, J_{C-P} = 63.1 Hz, Ph, PPh_3) 125.9 (NCN). $^{31}P\{^1H\}$ NMR ($CDCl_3$, 121.5 MHz, 294 K) δ 30.46. ^{19}F NMR ($CDCl_3$, 282.3 MHz, 294 K) δ −80.8. ESI^+: *m/z* = 541.0 $[M-OTf]^+$. Anal. Calcd. (%) for $C_{23}H_{21}F_3N_2O_3PSAu$: C, 40.01; H, 3.07; N, 4.06. Found: C, 40.35; H, 3.23; N, 4.11.

Preparation of compound 2. A flask was charged with 42 mg (0.619 mmol) of imidazole, 20 mL de CH_2Cl_2 and 610.8 mg (0.4125 mmol) of $[O(AuPPh_3)_3]BF_4$. After 2 h of stirring, the mixture changed from colorless to pale-yellow. Then, the solution was evaporated to minimum volume under vacuum, and compound **2** was precipitated with diethyl ether as a beige solid.

$[I(AuPPh_3)_2H]BF_4$ (**2**). Yield: 0.5070 g (76%). ^1H NMR ($CDCl_3$, 400 MHz, 294 K) δ 7.90 (s, 1H, H2, Im), 7.60-7.55 (m, 30H, Ph, PPh_3), 7.20 (s, 2H, H4-H5, Im). $^{13}C\{^1H\}$-APT NMR ($CDCl_3$, 101 MHz, 294 K) δ 134.50 (d, $J_{C-P}=13$ Hz, Ph, PPh_3), 132.81 (d, $J_{C-P}=2$ Hz, Ph, PPh_3), 131.79 (NCN), 129.88 (d, $J_{C-P}=12$ Hz, Ph, PPh_3), 128.27 (d, $J_{C-P}=64$ Hz, Ph, PPh_3), 126.60 (C=C). NMR $^{31}P\{^1H\}$ ($CDCl_3$, 162 MHz, 294 K) δ 31.72. ^{19}F NMR ($CDCl_3$, 376.5 MHz, 294 K) δ −148.2. MALDI$^+$ mass: $m/z=985.1$ [M-BF_4]$^+$, 527.1 [M–Au(PPh_3)+H-BF_4]$^+$. Anal. Calcd. (%) for $C_{39}H_{33}BF_4N_2P_2Au_2$: C, 43.68; H, 3.10; N, 2.61. Found: C, 43.51; H, 3.30; N, 2.43.

Computational details: Computational results were obtained by using the DFT functional ωB97XD[32] with the D2 Grimme dispersion correction[37] as implemented in Gaussian 16.[38] The SDD basis set with ECP for Au and the 6–311++G(d,p) basis set for other atoms were used. Solvents were described using the SMD continuum solvation model.[39] pKa's were determined using a direct approach at the same level of theory,[40] which has been used before in several systems.[41–43] Natural Bond Orbital analysis, which provided mechanistic details of the activation reaction, was performed by using the NBO Version 3.1[44] implemented in Gaussian 16. Bond properties were determined according to the formalism of reference.[32]

Crystallographic data. Crystals were mounted in inert oil on glass fibers and transferred to the cold gas stream of an Xcalibur Oxford Diffraction diffractometer equipped with low-temperature attachments. Data were collected using monochromated Mo Kα radiation (λ=0.71073 Å). The scan type was ω. Absorption corrections based on multiple scans were applied using spherical harmonics implemented in SCALE3 ABSPACK scaling algorithm.[45] The structures were solved with the ShelXS structure solution program using direct methods and by using Olex2 as the graphical interface.[46] Deposition Number(s) 2334416 (for **1**) contains the supplementary crystallographic data for this paper. These data are provided free of charge by the joint Cambridge Crystallographic Data Centre and Fachinformationszentrum Karlsruhe Access Structures service.

Electrochemical details: Cyclic voltammetry (CV) and Osteryoung square wave voltammetry (OSWV) were performed at room temperature in dry acetonitrile as solvent using tetra-n-butylammonium hexafluorophosphate (NBu_4PF_6 0.1 m) as supporting electrolyte. A glassy carbon electrode was used as the working electrode, an Ag wire as a pseudo-reference, and a Pt wire as the counter- electrode. The redox potentials were referenced to the internal ferrocene/ferrocenium couple (Fc/Fc^+).

Acknowledgements

The authors are deeply thankful to the Vicerrectoría de Investigaciones and the Centro de Excelencia en Nuevos Materiales (CENM) from the Universidad del Valle for the financial support. The authors also thank project PID2022-136861NB-I00 funded by MICIU/AEI/10.13039/501100011033 and Gobierno de Aragón (Research Group E07_23R) for financial support of our research.

Conflict of Interests

The authors declare no conflict of interest.

Data Availability Statement

The data that support the findings of this study are available in the supplementary material of this article.

Keywords: *N*-Heterocyclic carbenes · Gold complexes · Imidazolium Salts · Migration reactions · Computational study

[1] S. Nayak, S. L. Gaonkar, *ChemMedChem* **2021**, *16*, 1360–1390.
[2] M. N. Hopkinson, C. Richter, M. Schedler, F. Glorius, *Nature* **2014**, *510*, 485–496.
[3] S. Díez-González, N. Marion, S. P. Nolan, *Chem. Rev.* **2009**, *109*, 3612–3676.
[4] R. Visbal, M. C. Gimeno, *Chem. Soc. Rev.* **2014**, *43*, 3551–3574.
[5] M. N. Hopkinson, C. Richter, M. Schedler, F. Glorius, *Nature* **2014**, *510*, 485–496.
[6] S. Bellemin-Laponnaz, S. Dagorne, *Chem. Rev.* **2014**, *114*, 8747–8774.
[7] Y. Pan, X. Jiang, Y. M. So, C. T. To, G. He, *Catalysts* **2020**, *10*, DOI 10.3390/catal10010071.
[8] O. Kühl, *Chem. Soc. Rev.* **2007**, *36*, 592–607.
[9] H. V. Huynh, *Chem. Rev.* **2018**, *118*, 9457–9492.
[10] H. Jacobsen, A. Correa, A. Poater, C. Costabile, L. Cavallo, *Coord. Chem. Rev.* **2009**, *253*, 687–703.
[11] D. J. Nelson, S. P. Nolan, *Chem. Soc. Rev.* **2013**, *42*, 6723–6753.
[12] R. Bhatia, J. Gaur, S. Jain, A. Lal, B. Tripathi, P. Attri, N. Kaushik, *Mini-Rev. Org. Chem.* **2013**, *10*, 180–197.
[13] K. M. Hindi, M. J. Panzner, C. A. Tessier, C. L. Cannon, W. J. Youngs, *Chem. Rev.* **2009**, *109*, 3859–3884.
[14] O. Schuster, L. Yang, H. G. Raubenheimer, M. Albrecht, *Chem. Rev.* **2009**, *109*, 3445–3478.
[15] L. Benhamou, E. Chardon, G. Lavigne, S. Bellemin-Laponnaz, V. César, *Chem. Rev.* **2011**, *111*, 2705–2733.
[16] M. Brill, J. Díaz, M. A. Huertos, R. López, J. Pérez, L. Riera, *Chem. A Eur. J.* **2011**, *17*, 8584–8595.
[17] M. A. Huertos, J. Pérez, L. Riera, J. Díaz, R. López, *Chem. A Eur. J.* **2010**, *16*, 8495–8507.
[18] G. Sini, O. Eisenstein, R. H. Crabtree, *Inorg. Chem.* **2002**, *41*, 602–604.
[19] J. Ruiz, B. F. Perandones, *J. Am. Chem. Soc.* **2007**, *129*, 9298–9299.
[20] J. Ruiz, D. Sol, J. F. Van der Maelen, M. Vivanco, *Organometallics* **2017**, *36*, 1035–1041.
[21] J. W. Runyon, O. Steinhof, H. V. R. Dias, J. C. Calabrese, W. J. Marshall, A. J. Arduengo, *Aust. J. Chem.* **2011**, *64*, 1165–1172.
[22] A. J. Arduengo, H. V. R. Dias, R. L. Harlow, M. Kline, *J. Am. Chem. Soc.* **1992**, *114*, 5530–5534.
[23] A. Johnson, M. C. Gimeno, *Chem. A Eur. J.* **2020**, *26*, 11256–11265.
[24] M. C. Gimeno, A. Laguna, *Chem. Soc. Rev.* **2008**, *37*, 1952–1966.
[25] N. V. Tzouras, F. Nahra, L. Falivene, L. Cavallo, M. Saab, K. Van Hecke, A. Collado, C. J. Collett, A. D. Smith, C. S. J. Cazin, S. P. Nolan, *Chem. A Eur. J.* **2020**, 4515–4519.
[26] M. A. Rosero-Mafla, J. Zapata-Rivera, M. C. Gimeno, R. Visbal, *Molecules* **2022**, *27*, 8289.
[27] A. Trommenschlager, F. Chotard, B. Bertrand, S. Amor, L. Dondaine, M. Picquet, P. Richard, A. Bettaïeb, P. Le Gendre, C. Paul, C. Goze, E. Bodio, *Dalton Trans.* **2017**, *46*, 8051–8056.
[28] S. Tsuzuki, A. Fujii, *Phys. Chem. Chem. Phys.* **2008**, *10*, 2584–2594.
[29] T. L. Amyes, S. T. Diver, J. P. Richard, F. M. Rivas, K. Toth, *J. Am. Chem. Soc.* **2004**, *126*, 4366–4374.
[30] J. C. Garrison, W. J. Youngs, *Chem. Rev.* **2005**, *105*, 3978–4008.
[31] K. B. Wiberg, *Tetrahedron* **1968**, *24*, 1083–1096.
[32] A. Moyano, M. A. Pericas, E. Valenti, *J. Org. Chem.* **1989**, *54*, 573–582.
[33] G. S. Hammond, *J. Am. Chem. Soc.* **1955**, *77*, 334–338.
[34] G. R. Fulmer, A. J. M. Miller, N. H. Sherden, H. E. Gottlieb, A. Nudelman, B. M. Stoltz, J. E. Bercaw, K. I. Goldberg, *Organometallics* **2010**, *29*, 2176–2179.
[35] A. N. Nesmeyanov, E. G. Perevalova, Y. T. Struchkov, M. Y. Antipin, K. I. Grandberg, V. P. Dyadhenko, *J. Organomet. Chem.* **1980**, *201*, 343–349.
[36] R. Uson, A. Laguna, J. L. Spencer, D. G. Turner, *Inorg. Synth.* **1982**, *21*, 71–74.
[37] S. Grimme, *J. Comput. Chem.* **2006**, *27*, 1787–1799.
[38] D. J. Frisch, M. J. Trucks, G. W. Schlegel, H. B. Scuseria, G. E. Robb, M. A. Cheeseman, J. R. Scalmani, G. Barone, V. Petersson, G. A. Nakatsuji, H. Li,

Research Article
doi.org/10.1002/ejic.202400108

X. Caricato, M. Marenich, A. V. Bloino, J. Janesko, B. G. Gomperts, R. Mennucci, B. Hratch, *Gaussian 16, Revis. B.01*. **2016**.
[39] A. V. Marenich, C. J. Cramer, D. G. Truhlar, *J. Phys. Chem. B* **2009**, *113*, 6378–6396.
[40] B. Thapa, H. B. Schlegel, *J. Phys. Chem. A* **2016**, *120*, 5726–5735.
[41] S. Dhers, A. Mondal, D. Aguilà, J. Ramírez, S. Vela, P. Dechambenoit, M. Rouzières, J. R. Nitschke, R. Clérac, J.-M. Lehn, *J. Am. Chem. Soc.* **2018**, *140*, 8218–8227.
[42] M. A. Rosero-Mafla, J. I. Castro, N. E. Sánchez, C. A. Mujica-Martinez, M. N. Chaur, *ChemistrySelect* **2020**, *5*, 7685–7694.
[43] D. Madroñero, C. A. Mujica-Martinez, A. Vázquez, *RSC Adv.* **2021**, *11*, 33235–33244.
[44] E. D. Glendening, A. E. Reed, J. E. Carpenter, F. Weinhold, *NBO Version 3.1* **2003**.
[45] Agilent Technologies, *CrysAlis PRO* **2011**.
[46] O. V. Dolomanov, L. J. Bourhis, R. J. Gildea, J. A. K. Howard, H. Puschmann, *J. Appl. Crystallogr.* **2009**, *42*, 339–341.

Manuscript received: February 26, 2024
Revised manuscript received: April 12, 2024
Accepted manuscript online: April 12, 2024
Version of record online: ■■, ■■

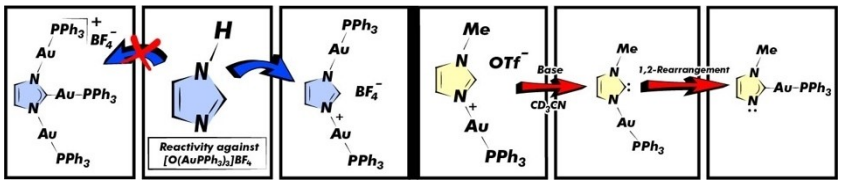

The reactivity of imidazole-based derivatives containing gold(I)-phosphane species towards the formation of imidazolium salts and the corresponding NHC-Au(I) complexes has been investigated. The results obtained indicate that the presence of the $[Au(PPh_3)]^+$ fragment promotes a great stabilization of imidazolium salts. However, this gold(I)-phosphane moiety is involved in a rearrangement process between the C- and N-bound species, associated to destabilization of Au-NHC complexes.

MSc. M. A. Rosero-Mafla, Prof. Dr. M. N. Chaur, Prof. Dr. C. A. Mujica-Martinez, Dr. V. Fernández-Moreira, Dr. J. Zapata-Rivera, Prof. Dr. M. C. Gimeno, Dr. R. Visbal**

1 – 9

Electronic Effect of the $[Au(PPh_3)]^+$ Fragment in the Stabilization of Imidazolium Salts and the Destabilization of NHCs